A Novel Approach to Borehole-Breathing Investigation in Naturally Fractured Formations

S. Baldino, S. Z. Miska, and **E. M. Ozbayoglu,** University of Tulsa

Summary

The occurrence of reversible mud losses and gains while drilling in naturally fractured formations (NFFs) is of primary concern. Borehole breathing can complicate the already difficult practice of fingerprinting the changes in the return-flow profile, hence undermining the reliability of kick detection. Issues can also derive from misdiagnosing a kick and attempting to kill a breathing well. The objective of this work is to correctly address the phenomenon and increase insights regarding its physical characterization. The fluid progressively flows in and out of fractures as a consequence of three mechanisms: bulk volume deformation, fluid compressibility, and fracture-aperture variation. To represent this complex scenario, a model involving a continuously distributed fracture network is developed. A time-dependent, 1D dual-poroelastic approach is coupled with a variable fracture aperture and a passive porous phase. Finite fracture network length is considered, and no limitation on the number of fractures is posed. The latter permits us to analyze long openhole sections intersecting several fissures, which is a more realistic approach than the available single-fracture models. The proposed model is able to quantify pressure distribution in fractures and pores, together with the flow rate entering or exiting the fractures. Furthermore, a useful application of the model is proposed by suggesting its application as a breathing discriminator during kick diagnosis. The shut-in drillpipe pressure (SIDPP), recorded from a real kick, has been compared with one caused by a simulated breathing case. Although the two SIDPPs show significant similarities, the correct modeling of breathing can help the identification of the major differences between a kick and breathing.

Introduction

Drilling operations become more and more challenging and complicated when dealing with high-temperature, high-pressure, and deepwater wells. This complexity has a significant effect on safety specifications and procedures, as well as on approval for expenditure costs. One of the primary concerns of these types of drilling environments is the narrow margin between the pore pressure and the fracture opening/initiation gradient. This might result in sizable drilling-fluid losses when drilling ahead, and fluid returns when circulation is stopped (Tare et al. 2001). The phenomenon is generally referred to as wellbore ballooning or breathing. Several causes of breathing events have been identified. Among them, there are radial expansion and contraction of tubular elements, such as risers, casing, and openhole (Gill 1989; Helstrup et al. 2001), and drilling-fluid thermal volumetric changes (Babu 1998; Karstad 1998; Aadnøy 2010; Yuan et al. 2016). Besides the mentioned causes, fracture-aperture variations should play a major role while drilling in fractured formations (Lavrov and Tronvoll 2005). If, while circulating the drilling mud, the bottomhole pressure increases to greater than the fracture opening/initiation pressure, drilling fluid will migrate into hydraulically connected fractures that intercept the well. As soon as circulation is stopped, the bottomhole pressure decreases and might cause the fractures to close. This occurs during a pumpoff period (connection, tripping, or flow-check operations) and might cause a sizable amount of mud to be returned back into the wellbore. Because no flow is expected to occur during pumpoff periods, the mud-flow return is more noticeable because it occurs rapidly. Wellbore-breathing misinterpretation might jeopardize kick-detection operations and lead to kick misdiagnosis. This can lead to different serious issues.

- A kick is wrongly assumed to be a mud-flow return. Such a scenario could result in well unloading, for example, through adaptive drilling techniques such as managed-pressure drilling (MPD). Consequently, the severity of the kick increases because more reservoir influx is allowed.
- On the other hand, potential safety issues can also derive from attempts to kill a breathing well when a kick is incorrectly diagnosed. Implementing unnecessary well-control practices is generally sufficient to cause existing fracture propagation and transform temporary losses into potential total losses. Undermining of wellbore integrity and increments of nonproductive time are the resulting consequences.

If borehole breathing is correctly identified, the most practical steps to contain it can be followed in the field (Power et al. 2003). Thus, it is important to correctly address the aforementioned phenomenon and increase the understanding of its physical characterization.

Literature Review

To date, the mechanisms behind wellbore breathing in NFFs have not been studied extensively. Tare et al. (2001) provided a comprehensive view on borehole breathing. Local geological characteristics, related natural fractures, wellbore design and trajectory, and drilling operational conditions have been listed as the major factors behind loss/gain events. Accordingly, breathing in NFFs is commonly observed under different circumstances. Among them are drilling through zones characterized by a limited fracture network, with negligible leakoff into the surrounding formation; drilling in deepwater environments with a narrow operating window between pore pressure and fracture gradient; and drilling long wells with high inclination angles (Tare et al. 2001). Several products and advanced drilling techniques have been used in attempts to prevent borehole breathing while drilling through natural and induced fractures (Ward and Clark 1998; Rosenberg and Gala 2011; Ochoa Lugo et al. 2011; Tirado Vargas et al. 2011). Given the importance of understanding the mechanisms behind drilling-fluid losses/gains in fractures, the industry and many researchers have made considerable efforts to model these phenomena. Dyke et al. (1995) first showed how to distinguish between losses through a porous matrix and those in natural

This paper (SPE 189661) was accepted for presentation at the IADC/SPE Drilling Conference and Exhibition, Fort Worth, Texas, USA, 6–8 March 2018, and revised for publication. Original manuscript received for review 15 March 2018. Revised manuscript received for review 20 August 2018. Paper peer approved 22 August 2018.

fractures. Lietard et al. (1996) derived curves for mud propagation vs. time for different hydraulic apertures using numerical solutions of the governing equations. Sanfillippo et al. (1997) used the diffusivity equation to model flow into natural fractures under a constant pressure difference. They assumed Newtonian muds and a nondeformable fracture with a constant aperture. No fluid exchange with the porous matrix was allowed. The model developed by Verga et al. (2000) makes use of the diffusivity equation and considers a constant-aperture approximation. Non-Newtonian fluids have been considered. As the output of the model, the fracture-aperture values were calculated and compared with those measured by electric imaging logs. Lavrov and Tronvoll (2003) developed a 1D linear model of mud loss into a single fracture and performed a sensitivity analysis to study the effects of different parameters on mud losses. Their model assumed Newtonian fluids. The latter model was extended to mud-loss events in radial coordinates (Lavrov and Tronvoll 2004) and non-Newtonian fluids. Moreover, a linearized fracture-deformation law was applied. When actual breathing mechanics is considered, all the available works are derived from a single-fracture model. Helstrup et al. (2003) studied wellbore breathing by means of a numerical poroelastic model for a single fracture. Lavrov and Tronvoll (2005) also studied borehole breathing. They modified their previous models by adopting the exponential deformation law for fracture-aperture variation, as proposed by Bruel et al. (1994). Lavrov and Tronvoll (2006) modeled the mud-loss events using a Cartesian-coordinate system and investigated the effects of fracture dimensions. Majidi et al. (2008, 2010) developed a mathematical model to study wellbore breathing and total losses as a function of the main fracture-controlling parameters (aperture, extension, and compliance) and fluid rheological properties. Ozdemirtas et al. (2009) conducted experimental tests and a numerical-model study, showing that fracture-surface roughness has a significant effect on the cumulative volume of mud gain/loss during borehole breathing. Ridley et al. (2013) developed a standard practice of creating a Horner plot to distinguish between wellbore breathing and actual reservoir influx by analyzing data from a shale-gas reservoir in the Eagle Ford Formation. Yuan et al. (2016) combined real-time pressure-while-drilling data and a transient simulator to help in distinguishing between drilling-fluid thermal expansion, wellbore breathing, and real kicks during flow check. Feng and Gray (2017) developed a numerical model to estimate fluid loss into a growing induced fracture driven by dynamic circulation pressure during drilling.

The Continuum Approach for a Fractured Porous Rock

Characterizing NFFs is not an easy task and requires multiple inputs from several disciplines. Numerous models were proposed in the early 1960s that considered NFFs as overlapping continua of homogeneous pores (matrix) and homogeneous fracture networks (Barenblatt and Zheltov 1960; Warren and Root 1963). Some researchers have recently moved away from this approach, and more-realistic NFF modeling has been proposed by discretizing the fracture network using an involved semianalytical model (Biryukov and Kuchuk 2012; Kuchuk and Biryukov 2015; Kuchuk et al. 2015). Most of the NFFs, and carbonate formations in particular, display a high degree of heterogeneity. Fracture properties vary throughout the formation, generally displaying a so-called power-law distribution (Belfield and Sovich 1995; Bour and Davy 1997). In addition, there are major problems with the dual-porosity model when it is used for NFF characterization: the inner (wellbore) boundary condition and the interporosity skin factor for the matrix blocks (Kuchuk et al. 2015).

The question is how to model breathing caused by interactions between the wellbore and natural/drilling-induced fractures. When wellbore breathing is involved, it appears convenient to distinguish between two apparent fluid phases: one that is mobile, occupying the fractures, and the other that is steady, occupying the pores. According to Belfield and Sovich (1995), the approximate average of fracture spacing in an NFF was found to be 0.3 m (1 ft), as shown in **Fig. 1.** In this sense, an openhole section of several hundred feet will most likely intercept more than just one or a few well-defined fractures. Keeping this in mind, it is here proposed to consider an ad hoc zone defined as the hydraulically connected field, after zone diversification given by Bear et al. (2012). The flow is assumed to occur in the fracture phase only, whereas the pore phase is treated as the passive continuum. Interphase exchange is not allowed. For each point within these continua, phase properties are averaged over a reference elementary volume (REV) sized, in length l, as the openhole section. If the REV is moved within the domain of interest (hydraulically connected field), a statistically significant number of hydraulically connected fractures should be encountered. This is supported by the fact that for a long openhole section of several hundred meters, the characteristic size of the REV guarantees $l \geq l_{\min} \gg \varsigma$, where for this case, ς is defined as the fracture spacing and translates to the scale of heterogeneity of the domain. Moreover, such an REV should be small enough to invalidate significant heterogeneity of the fractures involved in fluid transport. Hence, the vast majority of the fractures in that domain will most likely be characterized by homogenized properties (spacing, aperture, orientation). The system ends up being dual porosity/single permeability. Interaction between the porous matrix and the network of fractures will be limited to a poromechanical response only. Automatically, the ill-defined inner-boundary condition, according to the problem at hand, reduces to the forms

$$p_m(a,t) = p_w, \quad m = 1,2 (1 = \text{fractures}, 2 = \text{pores}), \quad t > 0,$$
$$r\frac{\partial p_1(r,t)}{\partial r}\bigg|_{r=a} = q \text{ and } r\frac{\partial p_2(r,t)}{\partial r}\bigg|_{r=a} = 0, \; t > 0. \qquad (1)$$

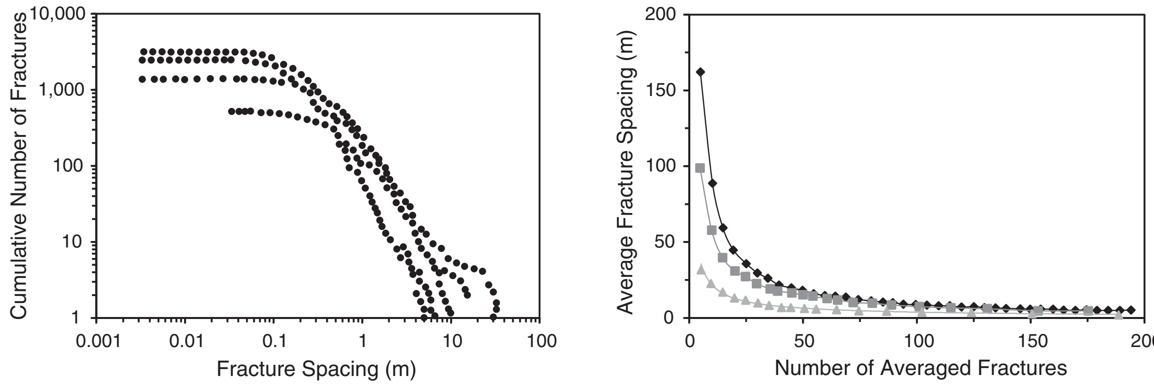

Fig. 1—Variation of fracture spacing as a function of the number of fractures, after Belfield and Sovich (1995).

Similarly, the interporosity skin factor ceases to be a problem because the flow occurs only through the fractures, given that the exceedingly short time frame of breathing does not allow for significant Darcy's flow through the pores. Moreover, the mud might as well generate an impermeable layer (or an interfacial mudcake) between the fracture walls and the porous block, thus enhancing further isolation of the two phases.

Dual-Porosity/Single-Permeability Model

When a single-porosity/single-permeability poroelastic model is considered, the theory developed by Terzaghi (1923), Biot (1941, 1956), and Biot and Willis (1957) represents the main foundation. The extension of this theory to dual-porosity systems has been proposed by several authors, and a solution to the borehole problem was provided as well (Aifantis 1979; Wilson and Aifantis 1982; Khaled et al. 1984; Valliappan and Khalili-Naghadeh 1990; Elsworth and Bai 1992; Berryman and Wang 1995; Bai et al. 1999; Abousleiman and Nguyen 2005).

Equilibrium Equations. To begin with, the equilibrium of forces acting on the REV is exactly the same as that derived for classical elasticity in the absence of inertia and body forces (Sadd 2009),

$$\sigma_{ij,j} = \overline{0}. \quad \ldots\ldots (2)$$

Where the index notation is adopted, a comma and following subscripts indicate differentiation with respect to spatial coordinates, whereas repeating indices imply summation over the range of the indices. The conservation of mass is described by Eq. 3, which includes the well-known continuity requirements for fluid phases $m = 1, 2$ (Aifantis 1979),

$$\frac{\partial \zeta_m}{\partial t} + \frac{\partial q_i^{(m)}}{\partial x_i} = 0. \quad \ldots\ldots (3)$$

The subscript (or parenthetical superscript) 1 denotes the fractures, whereas 2 refers to the pores. The fluid increment of each phase is referred to as ζ_m, whereas $q_i^{(m)}$ is the fluid-volume flux of each phase. In Eq. 3, no source term accounting for interporosity communication is considered (see the justifications discussed previously). The conservation of linear momentum for the pore and fracture phases is given by Eqs. 4 and 5, respectively.

$$q_i^{(2)} = -\frac{k_2}{\mu}\frac{\partial p_2(\overline{x}, t)}{\partial x_i}. \quad \ldots\ldots (4)$$

Eq. 4 is the so-called Darcy's law, and represents momentum balance for the fluid phase $m = 2$. k_2 represents the permeability of the matrix phase (which is considered as zero), μ is the dynamic viscosity of the pore fluid, and p_2 is the matrix pore pressure. Regarding flow through the fractures, a slight deviation from Darcy's permeability is proposed to provide a better representation of the hydrodynamics of flow into fissures. Reynold's lubrication theorem is applied (Zimmerman and Bodvarsson 1996),

$$q_i^{(1)} = -\frac{k_1(\overline{x}, t)}{\mu}\frac{\partial p_1(\overline{x}, t)}{\partial x_i} = -\frac{h^3(\overline{x}, t)}{12\varsigma\mu}\frac{\partial p_1(\overline{x}, t)}{\partial x_i}, \quad \ldots\ldots (5)$$

where $h(\overline{x}, t)$ represents the fracture aperture. More details will be given in the following subsection.

Constitutive Equations. Regarding the mechanical response, both stresses and strains cannot be described independently for each phase. This means that on the REV boundary, stresses and strains have to be expressed in a superimposed fashion. Assuming homogeneity and isotropy of the fractured porous medium, the constitutive equations governing the response of the porous or fractured phase can be expressed as (Aifantis 1979)

$$\sigma_{ij} = 2G\varepsilon_{ij} + 2G\frac{\nu}{1-2\nu}\varepsilon_{kk}\delta_{ij} - \sum_{m=1}^{2}\overline{\alpha}_m p_m \delta_{ij}. \quad \ldots\ldots (6)$$

The material properties G and v are the shear modulus and Poisson's ratio, respectively, whereas ε_{kk} and ε_{ij} are the volumetric strain and strain-tensor components, respectively. $\overline{\alpha}_1$ and $\overline{\alpha}_2$ are referred to as the generalized Biot and Willis (1957) parameters, as defined in Eq. A-2. It is then necessary to formulate constitutive equations that express the coupling between the state of deformation and the fluid flow in the two phases. According to the constitutive framework proposed by Berryman and Wang (1995), Eq. 7 is used to express the increment of fluid content in the two phases, ζ_m, as unique functions of pressures and volumetric strain, ε_{kk}.

$$\begin{aligned}\zeta_1 &= \overline{\alpha}_1\varepsilon_{kk} + \frac{\overline{\alpha}_1}{B_{u1}K_{u1}}p_1 + \left(a_{23} - \frac{\overline{\alpha}_1\overline{\alpha}_2}{K}\right)p_2,\\ \zeta_2 &= \overline{\alpha}_2\varepsilon_{kk} + \frac{\overline{\alpha}_2}{B_{u2}K_{u2}}p_2 + \left(a_{23} - \frac{\overline{\alpha}_1\overline{\alpha}_2}{K}\right)p_1. \end{aligned} \quad \ldots\ldots (7)$$

More details on the material coefficients in Eq. 7 are given in Appendix A. It shall be noted that the presence of the cross-coupling terms at the far-right-hand side of Eq. 7 can be neglected (Berryman and Wang 1995).

Field Equations. It is now possible to define the field equations for the problem. It is first worthy to note that the strain-displacement relationship, as derived for classical elasticity, still holds.

$$\varepsilon_{ij} = \frac{1}{2}(u_{i,j} - u_{j,i}). \quad \ldots\ldots (8)$$

Combining the equilibrium equation (Eq. 2) and the constitutive equation (Eq. 6) for the porous/fractured medium, and then using Eq. 8, leads to

$$G\nabla^2 u_i + (\lambda + G)\nabla \cdot (\nabla u_i) = \overline{\alpha}_1 \frac{\partial p_1}{\partial x_i} + \overline{\alpha}_2 \frac{\partial p_2}{\partial x_i}. \quad (9)$$

Eq. 9 is referred to as the Navier equation, and λ is one of the Lamé parameters (Sadd 2009). Then, by combining the continuity requirements with Darcy's law and the constitutive relationship (Eq. 7) with cross-coupling terms being zero, we obtain

$$\frac{k_1}{\mu}\nabla^2 p_1 = \frac{\overline{\alpha}_1}{B_{u1}K_{u1}}\frac{\partial p_1}{\partial t} + \overline{\alpha}_1 \frac{\partial \varepsilon_{kk}}{\partial t},$$
$$0 = \frac{\overline{\alpha}_2}{B_{u2}K_{u2}}\frac{\partial p_2}{\partial t} + \overline{\alpha}_2 \frac{\partial \varepsilon_{kk}}{\partial t}. \quad (10)$$

In particular, the interest is in modeling the flow-deformation response of a double-porosity medium that is defined by a finite fluid-discharge region of length b, surrounding a wellbore of radius a. In our case, interest shall fall on the region defined by the damaged radius of the hydraulically connected fractures, as shown schematically in **Fig. 2.**

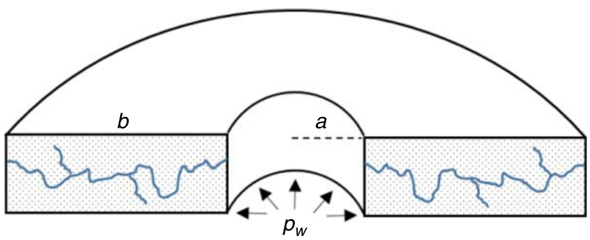

Fig. 2—Schematic cross-sectional view of a small portion of open hole, with finite fracture network length fractures.

It shall be noted that when a vertical well intercepts a finite-conductivity fracture with an inclination angle lower than 90°, a radial-flow regime is usually observed (Kuchuk et al. 2015). The latter is under the assumption of high contrast between the matrix and fracture permeabilities. This applies to the present case because the permeability of the pores does not have an active role in drilling-fluid migration. Thus, the following assumptions apply.

1. The fractures are initially empty, or otherwise saturated with fluid that has the same properties as the wellbore fluid.
2. Each continuum can be considered homogeneous and isotropic.
3. Flow and elastic bulk deformations are in the radial direction only.
4. Flow into fractures is laminar, and the fluid is considered Newtonian.
5. The fracture aperture is considered as a constant to derive the analytical solution first.
6. Plane-strain conditions apply.
7. The wellbore is vertical, and the problem is axially symmetric (isotropic in-situ horizontal stresses).
8. No fracture propagation.

Analytical Modeling

Eq. 9, for three directions, and Eq. 10 represent a system of five equations with five unknowns (u, v, w, p_1, p_2), where u, v, and w are the solid displacement in the radial, tangential, and vertical directions, respectively. The system can be further simplified under the special circumstances given previously:

$$(\lambda + 2G)\frac{\partial}{\partial r}\left[\frac{1}{r}\frac{\partial}{\partial r}(ru)\right] = \overline{\alpha}_1 \frac{\partial p_1}{\partial r} + \overline{\alpha}_2 \frac{\partial p_2}{\partial r}, \quad (11a)$$

$$\frac{k_1}{\mu}\frac{1}{r}\left[\frac{\partial}{\partial r}\left(r\frac{\partial p_1}{\partial r}\right)\right] = \frac{\overline{\alpha}_1}{B_{u1}K_{u1}}\frac{\partial p_1}{\partial t} + \overline{\alpha}_1 \frac{\partial}{\partial t}\left[\frac{1}{r}\frac{\partial}{\partial r}(ru)\right], \quad (11b)$$

$$\frac{\overline{\alpha}_2}{B_{u2}K_{u2}}\frac{\partial p_2}{\partial t} + \overline{\alpha}_2 \frac{\partial}{\partial t}\left[\frac{1}{r}\frac{\partial}{\partial r}(ru)\right] = 0, \quad (11c)$$

Eq. 11 is a system of coupled partial-differential equations with constant coefficients (fracture aperture is considered as constant for now). The first step is to decouple Eq. 11. For this purpose, we integrate Eq. 11a once as

$$\frac{1}{r}\frac{\partial}{\partial r}(ru) = \frac{\overline{\alpha}_1}{(\lambda + G)}p_1 + \frac{\overline{\alpha}_2}{(\lambda + G)}p_2 + \frac{g(t)}{(\lambda + G)}. \quad (12)$$

In Eq. 12, $g(t)$ is an integration constant that is a function of time in the most general case. Determination of the asymptotic values of the integration constant $g(t)$ can be performed for dual porosity in a way similar to that proposed by Rice and Cleary (1976), which is performing an undrained and drained analysis on an externally jacketed rock. Nevertheless, the presence of $g(t)$ can complicate the solution of Eq. 11. It can be shown that for $b/a \geq 10$, the temporal effect of the integration constant on the stress distribution can be

neglected (Detournay and Carvalho 1989; Schmitt et al. 1993). Moreover, assuming our reservoir extends to infinity (while being finite on the radial-fluid-discharge length), it is possible to use the approximation (Rice and Cleary 1976)

$$g(t) \approx 0. \quad \ldots\ldots (13)$$

Now, substituting Eq. 12 into Eqs. 11b and 11c, after some algebraic manipulations, we obtain

$$\frac{1}{C_{11}}\frac{\partial p_1}{\partial t}+\frac{1}{C_{12}}\frac{\partial p_2}{\partial t}=\frac{1}{r}\left[\frac{\partial}{\partial r}\left(r\frac{\partial p_1}{\partial r}\right)\right], \quad \ldots\ldots (14a)$$

$$\frac{1}{C_{21}}\frac{\partial p_1}{\partial t}+\frac{1}{C_{22}}\frac{\partial p_2}{\partial t}=0, \quad \ldots\ldots (14b)$$

where the coefficients have been contracted as

$$\frac{1}{C_{11}}=\frac{h^3}{12\mu\varsigma\left[\frac{\overline{\alpha}_1}{B_{u1}K_{u1}}+\overline{\alpha}_1^2/(\lambda+G)\right]};$$

$$\frac{1}{C_{12}}=\frac{h^3}{12\mu\varsigma[\overline{\alpha}_1\overline{\alpha}_2/(\lambda+G)]};$$

$$\frac{1}{C_{12}}=\frac{\overline{\alpha}_2\overline{\alpha}_1}{(\lambda+G)};$$

$$\frac{1}{C_{22}}=\frac{\overline{\alpha}_2}{B_{u2}K_{u2}}+\frac{\overline{\alpha}_2^2}{(\lambda+G)}. \quad \ldots\ldots (15)$$

Eq. 14 can be solved independently from the deformation field. Before moving forward, the initial and boundary conditions applicable to the system need to be defined.

$$p_1(a,t)=p_w, \ t>0, \quad \ldots\ldots (16a)$$

$$r\frac{\partial p_1(r,t)}{\partial r}\bigg|_{r=b}=0, \ t>0, \quad \ldots\ldots (16b)$$

$$p_1(r,0)=p_{10}, \quad p_2(r,0)=p_{20}, \ t=0. \quad \ldots\ldots (16c)$$

At the wellbore radius, the imposed pressure equals the wellbore pressure. On the other hand, the conditions imposed in Eq. 16b make sure that no flow is permitted at the fracture tip. To solve the partial-differential-equation system (Eq. 14), a specific finite Hankel's transform pair is defined according to the applicable boundary conditions (Cinelli 1965). The technique at the base of the proposed solution consists of solving the Sturm-Liouville problem for the boundary-value problem at hand (Cinelli 1965; Sneddon 1995). With the detailed derivations given in Appendix B, the solution for the pressure distribution in the fractures and pores can be derived as

$$\begin{cases} p_1(r,t)=p_w+\pi(p_{10}-p_w)\sum_{n=1}^{\xi_n}\frac{J_1(\xi_n b)J_0(\xi_n a)}{[J_0^2(\xi_n a)-J_1^2(\xi_n b)]}U(\xi_n r)e^{-C_{11}^*\xi_n^2 t}, \\ p_2(r,t)=\pi\sum_{n=1}^{\xi_n}\frac{J_1(\xi_n b)J_0(\xi_n a)}{[J_0^2(\xi_n a)-J_1^2(\xi_n b)]}U(\xi_n r)\left[\frac{C_{22}}{C_{21}}(1-e^{-C_{11}^*\xi_n^2 t})(p_{10}-p_w)+p_{20}\right]. \end{cases} \quad \ldots\ldots (17)$$

As can be seen, where flow takes place (i.e., in the fracture phase), the solution retains the same shape as the one derived by Muskat (1934). The only difference consists in the generalized consolidation coefficient C_{11}^* (see Appendix B). Given the assumption of flow taking place only in the fractures, the flow entering or leaving the fractures can be expressed as

$$Q(r,t)=\frac{2\pi H h_1^3}{12\varsigma\mu}\left(r\frac{\partial p_1}{\partial r}\right)\bigg|_a=\frac{2\pi^2 h_1^3 Ha}{12\varsigma\mu}(p_{10}-p_w)\sum_{n=1}^{\xi_n}\frac{J_1(\xi_n b)J_0(\xi_n a)}{J_0^2(\xi_n a)-J_1^2(\xi_n b)}U'(\xi_n a)e^{-C_{11}^*\xi_n^2 t}, \quad \ldots\ldots (18)$$

where $U'(\xi_n a)=\xi_n[J_1(\xi_n a)Y_1(\xi_n b)-Y_1(\xi_n a)J_1(\xi_n b)]$. If integration in time is performed, we can derive an expression for the cumulative fluid volume that is lost or gained.

$$V(r,t)=\int_0^t Q\mathrm{d}t=\frac{4\pi h_1^3 H}{12\mu\varsigma C_{11}^*}\left\{\sum_{n=1}^{\xi_n}\frac{{J_1}^2(\xi_n b)}{[J_0^2(\xi_n a)-J_1^2(\xi_n b)]{\xi_n}^2}-\sum_{n=1}^{\xi_n}\frac{{J_1}^2(\xi_n b)}{[J_0^2(\xi_n a)-J_1^2(\xi_n b)]{\xi_n}^2}e^{-C_{11}^*{\xi_n}^2 t}\right\}(p_{10}-p_w). \quad \ldots\ldots (19)$$

Eq. 19 has been obtained by the aid of Eq. B-22 (bottom) and some rearrangements. When no coupling is considered between deformation and fluid flow (i.e., C_{11}^* equals the classical hydraulic-diffusion coefficient), and the same inputs given in Van Everdingen and Hurst (1949) are used, we obtain a perfect match of the dimensionless cumulative volume "produced" using Eq. 19 **(Fig. 3).**

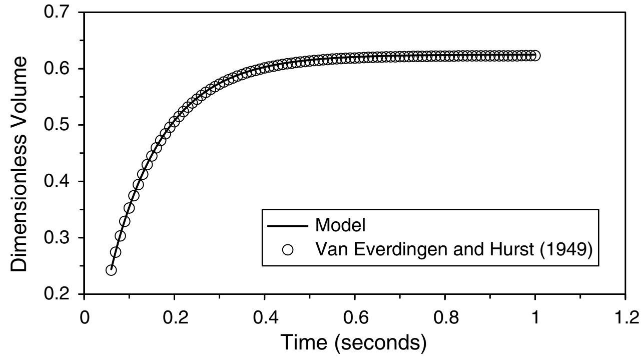

Fig. 3—Comparison between proposed model and Van Everdingen and Hurst (1949) solution.

Variable Fracture Aperture

To express the fracture permeability as a function of space and time, we can use the definition (Muskat 1949)

$$k_f(\bar{x},t)=\frac{h^2(\bar{x},t)}{12}. \quad (20)$$

Eq. 20 gives an expression for the permeability of a single fracture, idealized as two parallel planes where flow takes place under an imposed pressure gradient, and h refers to the fracture aperture. Now, considering a certain interval z, along which uniformly spaced planar fractures are assumed, we can state

$$k_1 z=k_f\left(\frac{z}{\varsigma}\right)h, \quad (21)$$

where k_1 is the mean permeability of the fractured rock. If ς is defined as the fracture spacing, z/ς is the number of fractures met from the top to the bottom of the considered stratum, and zh/ς is the combined thickness of all the fractures. If Eq. 20 is used in Eq. 21, a formulation of aperture-dependent permeability and porosity, for a fractured rock, is derived (Jones 1975) as

$$k_1=\frac{h^3(\bar{x},t)}{12\varsigma},$$
$$\phi_1=\frac{h(\bar{x},t)}{\varsigma}. \quad (22)$$

For this particular case, a constitutive equation governing the fracture-aperture variation will be needed. For our scope, the exponential relationship between fracture pressure and fracture aperture is adopted (Bruel et al. 1994).

$$\mathrm{d}h=h^*\exp\left\{\frac{-\gamma[\sigma_n-p_1(\bar{x},t)]}{3}\right\}, \quad (23)$$

where h^* (in in.) and γ (in psi^{-1}) represent the maximum fracture aperture preceding propagation and fracture compressibility, respectively. The normal stress is expressed by σ_n (in psi) and is a function of the fracture-inclination angle and in-situ stresses,

$$\sigma_n=\sigma_v\cos^2\alpha+\sigma_h\sin^2\alpha. \quad (24)$$

In Eq. 24, the horizontal stress σ_h is considered to be the minimum stress in the case of the anisotropic in-situ stress state, whereas α is the fracture-inclination angle with respect to the wellbore. It shall be noted that when drilling with conventional muds, with particle-size distribution as specified by *API SPEC 13A* (2010), complete bridging of induced and/or natural fractures cannot be achieved because of the larger values of fracture apertures. Special lost-circulation materials or loss-prevention materials should be used for this purpose (Lietard et al. 1996). The latter can be especially beneficial to mitigate or prevent wellbore breathing. However, if no care is taken on designing an appropriate loss-prevention material, the filter cake will only build around the porous matrix, with little influence on fractures. Another potential help can come from casing drilling. In that case, the smeared cuttings could help in bridging the fractures because they are plastered against the wellbore wall (Marbun et al. 2014).

Results Analysis

To obtain the pressure distribution in the fractures by also accounting for fracture-aperture variation, a numerical scheme has been implemented. The system is discretized in time and space as shown in **Fig. 4.**

To check the behavior of the model, the following results have been produced by analyzing two different rock formations: a compliant rock, Berea Sandstone, and a stiffer rock, Westerly Granite. Dual-porosity media are not easy to characterize. Thus, to have the most accurate values of the formation properties, several references have been studied and **Table 1** summarizes the data collected and the corresponding source of origin.

Berea Sandstone is considered the reference case, and scenarios with the following differences have been simulated:

- Case 1: Berea Sandstone.
- Case 2: Westerly Granite and operating conditions equal to Case 1.
- Case 3: Berea Sandstone and higher equivalent circulating density (ECD) (from 10.35 to 12 lbm/gal).
- Case 4: Berea Sandstone and lower viscosity (from 80 to 10 cp).

For all cases, three fracture inclinations have been tested (0, 45, and 75°, with 0° being a horizontal fracture intercepting the vertical well), while a fracture initial pressure (p_{10}) corresponding to 0.8 × ECD has been considered together with the wellbore data presented in **Table 2,** where ESD means equivalent static density.

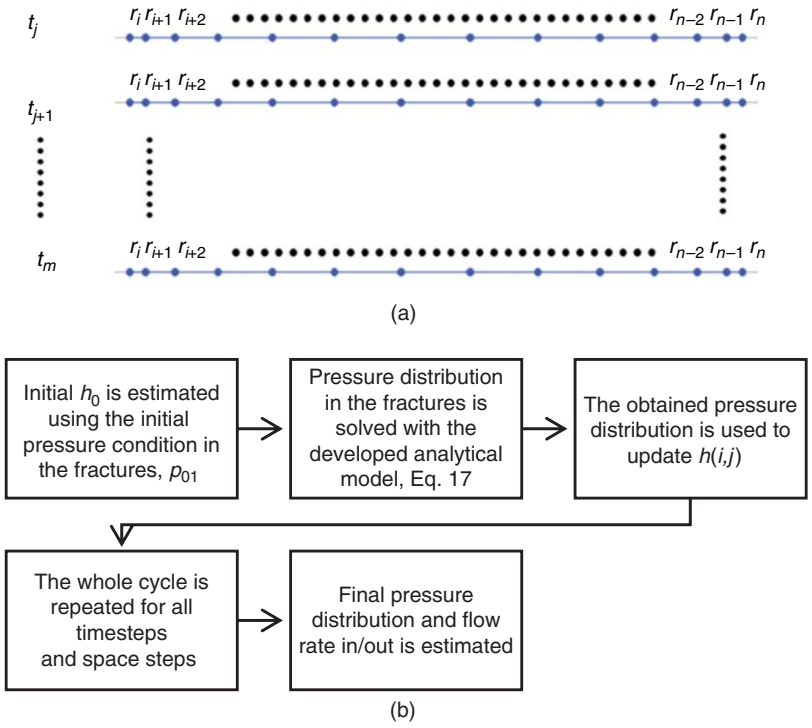

Fig. 4—(a) Domain discretization; (b) numerical scheme.

Parameter	Berea Sandstone	Westerly Granite
K_2 (psi)	$1.16\times10^{6*}$	$3.6\times10^{6*}$
v	0.20^{*}	0.25^{*}
b (ft)	12	12
α_2	0.78^{**}	0.45^{**}
K_f (psi)	2.9×10^{5}	2.9×10^{5}
h^* (in.)	1.5×10^{-2}	1.5×10^{-2}
B_2	0.551^{**}	0.810^{**}
ς (ft)	1	1
K_1 (psi)	$1.125\times10^{3\dagger}$	$1.27\times10^{4\dagger}$

* Rice and Cleary (1976)
** Cheng (2016)
† Elsworth and Bai (1992)

Table 1—Rock and system properties.

Well depth (ft)	8,200
ESD (lbm/gal)	10.0
ECD (lbm/gal)	10.35
Wellbore diameter (in.)	8.5
Openhole section (ft)	328
Virgin pore pressure (psi)	3,530
Overburden gradient (psi/ft)	1.0
Horizontal isotropic stress (psi)	4,641

Table 2—Vertical-wellbore data.

Case 1. To begin with, the mud-loss case while circulating has been simulated for Case 1. Shown in **Fig. 5,** the model is able to replicate the typical flow-rate exponential profile expected during breathing events (Lavrov and Tronvoll 2005; Majidi et al. 2008, 2015).

With reference to Fig. 5, some important observations can be made. Once the fluid has been compressed and the system deformed according to the imposed pressure inside the fractures, a decline is observed in the flow rate entering the fissures. Depending on the angle at which the fracture intercepts the well, different flow curves are obtained. As expected, the lower the fracture inclination, the higher the resistance to fracture opening. The latter is caused by the more pronounced effect of the overburden on the stress normal to the fracture plane (Eqs. 23 and 24). If the normal stress is larger, the resulting fracture aperture will be smaller, as will be the fracture's

effective permeability and porosity. Altogether, this results in a smaller volume of fluid lost over a larger amount of time, as shown in **Fig. 6.** For all three scenarios, the time frame is in line with that observed in the field (Ashley 2000). It is noted that 12 to 21 bbl lost is also a realistic range, on the same order of magnitude for average mud losses registered while drilling breathing wells (Ashley 2000). The corresponding results for the fluid-gain scenario are shown in Case 4, when the effect of fluid viscosity is analyzed. It can also be seen that changes in the fracture aperture are the major contribution to fluid losses in natural fractures. A plot of fracture aperture with pressure and inclination angle for Case 1 is shown in **Fig. 7.**

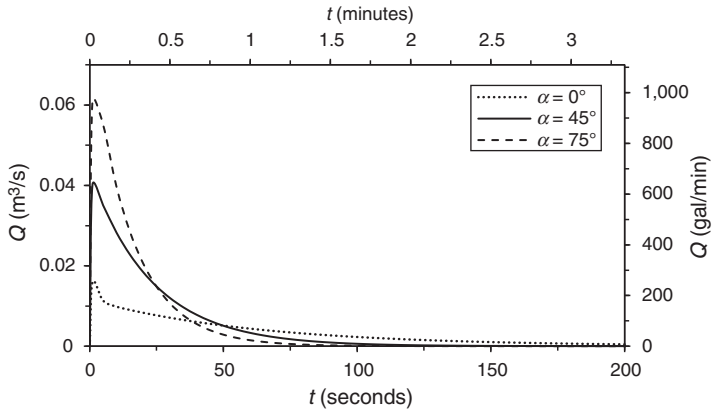

Fig. 5—Case 1: Flow rate entering the fractures for different fracture inclinations; $\gamma = 5.5\times10^{-4}$ psi^{-1}.

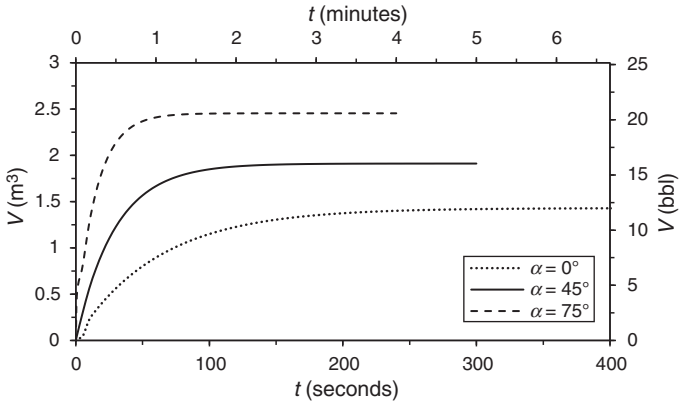

Fig. 6—Case 1: Total volume lost in the fractures for different fracture-inclination angles.

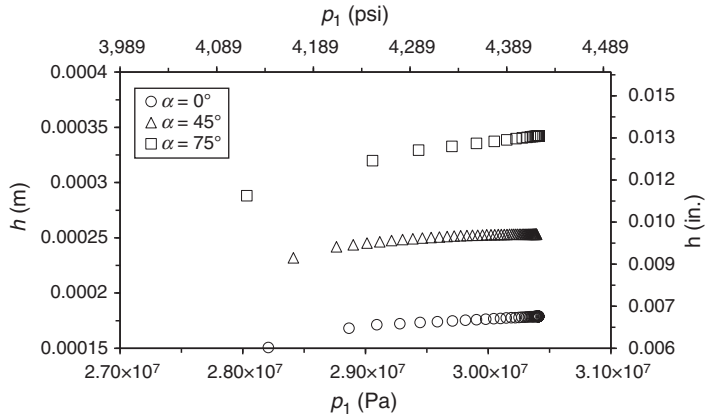

Fig. 7—Case 1: Fracture-aperture variation with pressure buildup at different fracture-inclination angles.

As expected, for horizontal fractures, the higher normal stress (equivalent to the overburden) causes the fracture aperture to be smaller in size and to grow with a much lower rate than in cases where the fracture is highly inclined, such as $\alpha = 75°$. The latter shows the highest values and growth rate of fracture width. This also affects the pressure buildup in the fissures, which will be faster for highly inclined fractures. This is caused by a faster fluid transport through larger apertures, and consequently greater fracture permeability. In **Fig. 8,** the pressure buildup in the fractures is plotted against the dimensionless radial distance from the wellbore, r/a. After 1 minute, for all cases, the fractures are already partially charged, with fracture pressure always being greater than the original formation pressure.

It is also of interest to analyze the behavior of the matrix pore pressure. This can be computed by means of Eq. 17 (bottom). It shall be noted that the pressure in the matrix, p_2, evolves solely because of the bulk deformation induced in the system by the change in the fracture pressure. The latter is a consequence of the assumption of a porous matrix not participating in the fluid transport. The spatial evolution of p_2 is plotted in **Fig. 9.**

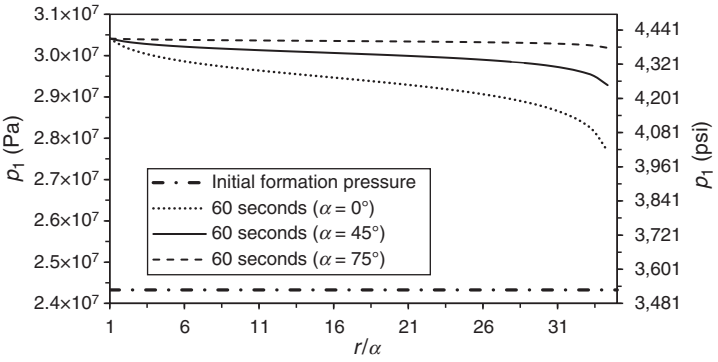

Fig. 8—Case 1: Fracture pressure buildup after 60 seconds for different fracture inclinations.

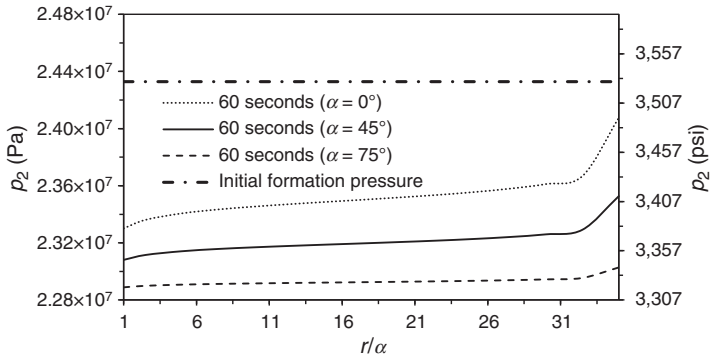

Fig. 9—Case 1: Matrix pore-pressure spatial evolution after 60 seconds for different fracture inclinations.

It is observed that the matrix pore pressure computed with the present model does not equal the wellbore pressure at $r = a$. This, in turn, is a consequence of the undrained response of the matrix phase. The virgin pore pressure in the pores is affected by the bulk deformation caused by the flow in the fractures. As the pressure in the fractures increases in the proximity of the well, the system enlarges, causing an expansion of the matrix pore space and resulting in a decrement of its pore pressure to less than the initial value (Fig. 9).

Case 2. When a much stiffer formation is considered (i.e., Westerly Granite), it is expected to have significantly lower values of bulk elastic deformation, together with higher resistance to fracture-aperture variation. This should lead toward a smaller amount of fluid stored in the fractures. This behavior is successfully represented by the proposed model and can be observed in **Fig. 10.**

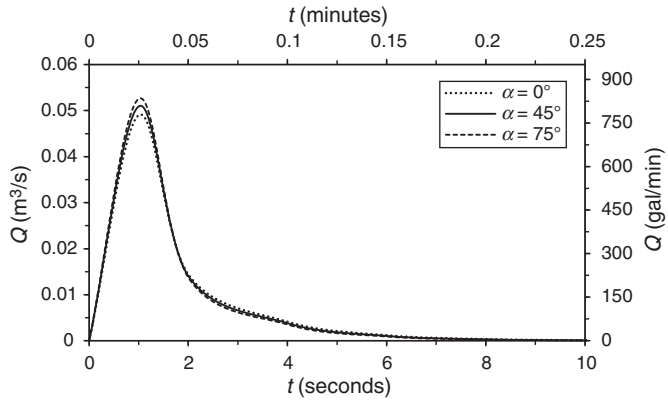

Fig. 10—Case 2: Flow rate entering the fractures for different fracture inclinations; $\gamma = 3.5\times10^{-5}$ psi^{-1}.

Fig. 10 shows an interesting behavior of mud invasion in a stiff formation. First, we notice the exceedingly short time needed to fill the fractures. After 10 seconds, there is almost no more flow in the fissured space. Moreover, the effect of fracture inclination is almost negligible (Lavrov and Tronvoll 2006). This is because a less-compliant fracture will resist further deformation, regardless of the normal stress acting on the fracture plane. Accordingly, the amount of lost volume is almost the same for the three cases considered, as shown in **Fig. 11.**

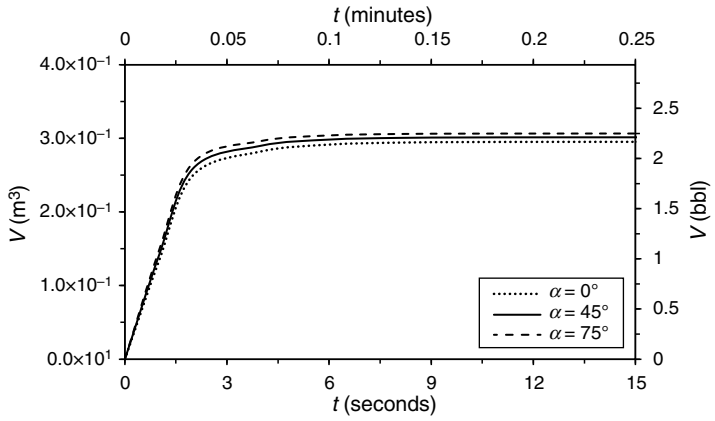

Fig. 11—Case 2: Total volume lost in the fractures for different fracture-inclination angles.

Similarly, with reference to the ESD value in Table 2, the corresponding results for the fluid-gain event can be computed. The mud-flow return and the total regained volume are plotted in **Figs. 12a and 12b,** respectively.

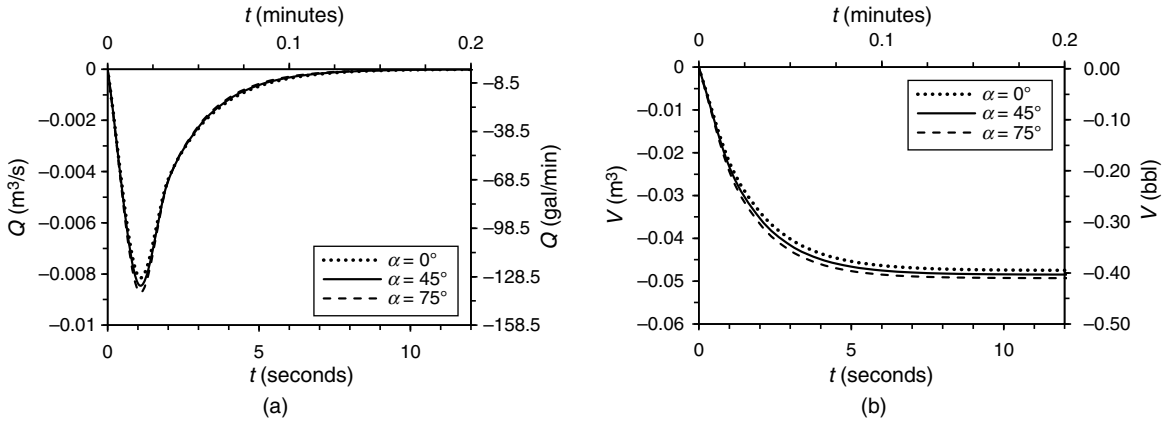

Fig. 12—Case 2: (a) Flow rate leaving the fractures and (b) total volume lost in the fractures for different fracture-inclination angles.

The behaviors of the mud-flow return and related total lost volume are similar to the loss scenario. The low fracture compressibility and the less-compliant characteristic of the granite caused the effect of fracture inclination to be almost negligible. One thing that should be noted is the magnitude of the fluid gain (Fig. 12b). In the case of fluid return, the driving force is the one resulting from the difference between ECD and ESD, which is a quite-limited drive if compared with the one behind the loss scenario. Hence, it explains the smaller volume returned to the wellbore.

Case 3. If the ECD is increased while everything else remains constant, this leads, as expected, to a significant increment of the flow rate that is lost into the fracture network, regardless of the fracture inclination. Not only is the rate of loss larger **(Fig. 13),** but also the time needed to fill the fissures has slightly decreased (this occurs toward the end of the loss event, where the mud flow related to higher ECD is, on average, approximately 40% smaller, although it is difficult to catch at sight from Fig. 13). The latter two observations can be explained by considering that higher ECD results in higher applied wellbore pressure. In turn, this causes larger fluid compression, higher elastic bulk deformations, and larger aperture variation. A correct design of the ECD in problematic zones can mitigate the magnitude of breathing. To design an efficient MPD plan, it can be beneficial to have this type of quantitative estimation of breathing-magnitude dependence on the mud weight. Also, a quantitative understanding of the influence of ECD on breathing magnitude can give an estimate of the expected reduction in fluid losses/gains before MPD implementation.

As mentioned, this causes a higher drilling-fluid volume stored in the fractures and larger values of fracture aperture. The latter is responsible for the slightly faster breathing event that can be observed at higher ECDs. A corresponding behavior is encountered if the total volume lost in the fractures is plotted against time, as shown in **Fig. 14.**

Case 4. Finally, to show the important effect of viscosity in breathing events, the mud-flowback phase is now simulated. Case 1 has been used again as a reference for flowback into the well, and then compared with Case 4 (lower viscosity). It is interesting to note in **Fig. 15** that a lower-viscosity fluid will cause a high peak in flow rate, followed by a fast decline to zero (for all fracture-inclination angles). The low-viscosity fluid is therefore squeezed out of the fractures much faster than in Case 1. On the other hand, a more-viscous fluid will not even get to one-half of that peak. To have a comprehensive understanding of all the possible flowback signatures of

breathing, the effect of viscosity is analyzed in **Fig. 16.** Fig. 16 shows a comparison between the total volume that entered the well (i.e., left the fractures) for Case 1 and Case 4 for all the fracture inclinations. Once again, the lower the viscosity, the faster the breathing event. On the other hand, the amount of the losses is not affected, and this is observed if enough time is allowed for the fractures to be depleted, in the case of higher viscosity.

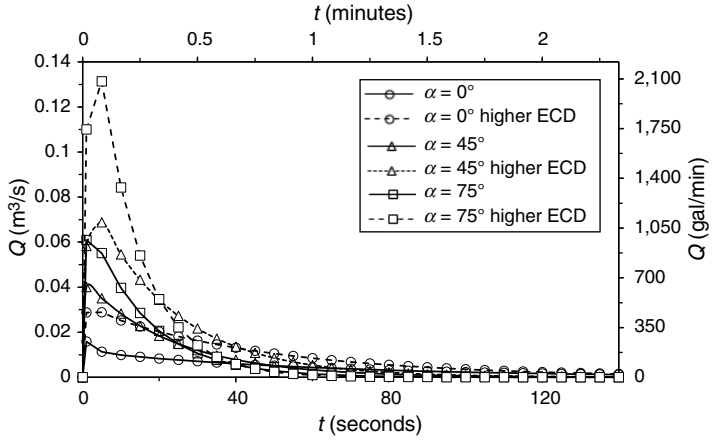

Fig. 13—Case 1 and Case 3 are compared. The effect of ECD on wellbore breathing is investigated.

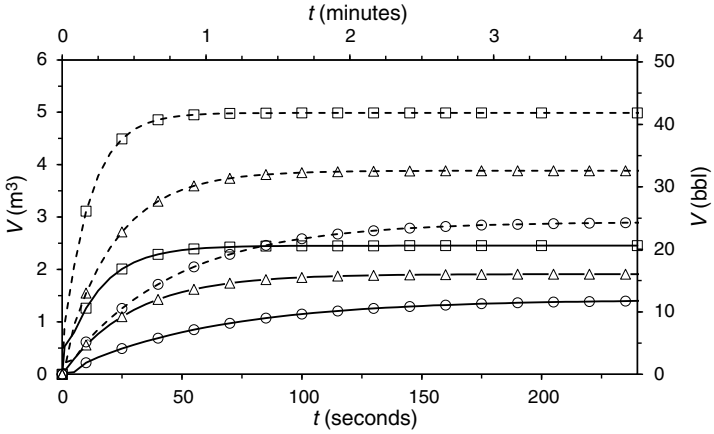

Fig. 14—Case 1 and Case 3 are compared. The effect of ECD on cumulative volume gained is compared. The same legend as Fig. 13 applies.

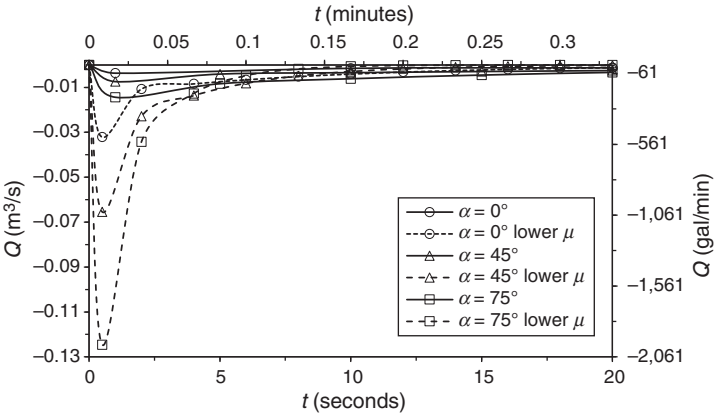

Fig. 15—Flow rate entering the well from the fractures for Cases 1 and 4 (different fracture inclinations).

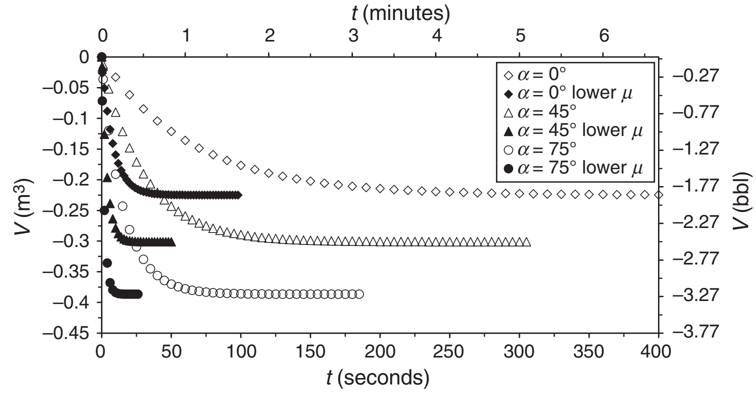

Fig. 16—Total-losses comparison between Cases 1 and 4 for different fracture inclinations.

Kick vs. Breathing: A Field Case

In this section, we discuss a comparison between pressure buildup in the drillpipe under shut-in conditions during both kick and breathing. Understanding the differences between these two events is important for both safety and drilling-efficiency reasons, as explained in the Introduction. To model the pressure buildup caused by wellbore shut-in during breathing, a simple mass balance in the wellbore is performed.

$$\Delta m = m_{\mathrm{in}} - m_{\mathrm{out}}. \quad (25)$$

When this is applied to well testing, it is possible to derive an equation that quantifies wellbore-storage effects caused by wellbore-fluid compressibility. If the same concept is applied in this case (considering drilling fluid, no formation fluid, and zero mass out), the equation for the shut-in pressure can be derived as

$$\frac{\mathrm{d}p_w}{\mathrm{d}t} = \frac{Q(t)}{V_{wb}\beta}, \quad (26)$$

where V_{wb} is the volume of the wellbore. If Eq. 26 is integrated with respect to time, the shut-in pressure buildup from the drilling fluid entering the wellbore can be found.

$$\Delta p_w = \int_0^t \frac{Q(t)}{V_{wb}\beta} \mathrm{d}t. \quad (27)$$

For comparison, a real set of SIDPP recorded at a kicking well in Louisiana will be used (Miska et al. 1998). The SIDPP buildup was recorded to estimate the stabilized pressure for a more effective selection of the killing-fluid density. The same input data as given by Miska et al. (1998) have been used, and a limestone rock has been chosen as the representative formation **(Tables 3 and 4).**

Parameter	Limestone
K_2 (psi)	3.3×10^6*
v	0.25*
b (ft)	35.0
α_2	0.7*
K_f (psi)	2.46×10^5
ς (ft)	1
B_2	0.42*
h^* (in.)	0.00787
K_1 (psi)	9.5×10^3
μ (cp)	55

* Hart and Wang (1995)

Table 3—Rock and system properties.

Well depth (ft)	14,075.0*
ECD (lbm/gal)	14.1*
Wellbore diameter (in.)	8.5*
ESD (lbm/gal)	13.5
Openhole section (ft)	500

* Miska et al. (1998)

Table 4—Vertical-wellbore data.

The simulated breathing event is shown in **Fig. 17** as the mud flow returned after stopping the circulation. Moreover, a wellbore shut-in after approximately 5 minutes has been simulated to compare this event with the wellbore response to a real kick.

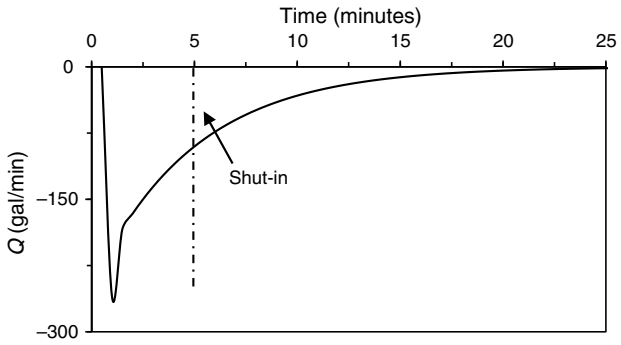

Fig. 17—Simulated mud-flow return and shut-in time for the Louisiana well under study.

With reference to **Fig. 18,** some interesting observations can be made. First, it can be seen that the SIDPPs show a similar growing trend at the very beginning (in this case, the breathing SIDPPs stabilize after approximately 6 minutes, whereas the kick SIDPP increases significantly until approximately 7.5 minutes). This explains the difficulties in discerning between a kick and a breathing event, particularly for exploration wells. However, the SIDPP during breathing shows a plateau, corresponding to the maximum Δp ($p_{ECD} - p_{ESD}$) achievable with the limited amount of drilling fluid that can enter the well. In this case, the maximum value of SIDPP has been calculated to be equal to 433 psi. In his detailed field observations, Gill (1989) described a reading of approximately 300 psi in the SIDPP just after pumpoff among the recurrent symptoms of wellbore ballooning. On the other side, the shut-in pressure resulting from the kick grows continuously because of the reservoir fluid accumulating in the annulus (compressibility effects) and the larger amount of fluid influx allowed (larger drive from the formation), often exceeding the $p_{ECD} - p_{ESD}$ difference. This type of comparison can be useful when performing fingerprinting of kicks. Moreover, a sharper pressure gradient, at the very beginning, can be observed if compared with the pressure gradient resulting from reservoir-fluid influx. This is because drilling muds are generally characterized by very low values of compressibility, whereas reservoir fluids often contain gas, which increases compressibility and in turn allows for smoother SIDPP increments. Nevertheless, the effect of a decreasing mud-flow rate that is entering the wellbore causes the pressure gradient, during breathing, to smoothen with time, and eventually to flatten. By collecting this type of information, a more well-informed decision can be taken on whether to apply well-control practices.

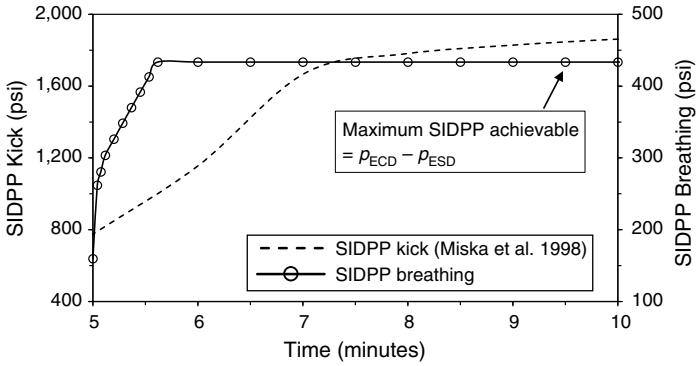

Fig. 18—SIDPP resulting from a kick [dashed line, after Miska et al. (1998)] and from breathing (continuous line).

Conclusions

1. The theory of consolidation has been shown to be a tool to describe the flow/deformation response of a fractured rock undergoing breathing events.
2. The proposed model is versatile and offers a margin of improvement over earlier models.
3. Breathing is sensitive to the dimensions of the fractures and to formation compliance.
4. The fracture-inclination angle with respect to the vertical wellbore has a more significant effect on breathing magnitude when drilling through compliant formations.
5. According to the results of the proposed model, the fluid viscosity significantly affects the time frame of fluid-loss/gain events.
6. The proposed model associates qualitative analysis with quantitative estimations of breathing events.
7. A correct modeling of breathing can help with understanding the major differences between kicks and breathing, as shown in the SIDPP comparison plot.
8. This model provides a semianalytical solution that shortens the computational time of a single-fracture model using numerical solutions (i.e., implicit or explicit finite difference).
9. Because of the last two points, this model can be implemented into automated kick-detection software as a breathing-discriminator tool (Tarr et al. 2016).

Nomenclature

a = wellbore radius, in.
b = damaged zone radius, ft
B_{um} = generalized Skempton coefficient of phase m
C_{11} = generalized consolidation coefficient, ft^2/min
G = shear modulus, psi
h = fracture aperture, in.
h^* = maximum attainable fracture aperture before propagation, in.
H = openhole-section length, ft
$H[f]$ = Hankel transform
J_v = first-kind Bessel functions, of order v
k_f = single-fracture permeability, md
k_m = phase permeability, md
K = bulk modulus, psi
K_f = fluid modulus, psi
K_{um} = generalized undrained bulk modulus of phase m, psi
L = matrix of eigenvectors
m_{in} = drilling-fluid mass entering the wellbore, lbm
m_{out} = drilling-fluid mass leaving the wellbore, lbm
p_m = phase pore pressure, psi
p_{mo} = initial phase pore pressure, psi
p_w = wellbore pressure, psi
$q_i^{(m)}$ = volumetric flux of phase m in i-direction, ft/min
Q = volumetric flow rate, gal/min
r = radial distance, ft
u_i = solid displacement, ft
v = Poisson's ratio
V = cumulative volume, bbl
V_{wb} = wellbore volume, bbl
Y_v = second-kind Bessel functions, of order v
α = fracture-inclination angle with respect to the wellbore, degrees
α_m = classical Biot and Willis (1957) coefficient of phase m
α_{23} = cross-storage coefficient, psi^{-1}
$\overline{\alpha}_m$ = generalized Biot and Willis (1957) coefficient of phase m
β = drilling-fluid compressibility, psi^{-1}
γ = fracture compressibility, psi^{-1}
δ_{ij} = Kronecker δ
ε_{ij} = strain-tensor components
ε_{kk} = normal-strain summation
ζ_m = increment of fluid content of phase m
λ = Lamé coefficient, psi
μ = fluid dynamic viscosity, cp
ν_m = phase-volume fraction
ξ_n = Hankel's variable, ft^{-1}
σ_h = minimum horizontal stress, psi
σ_{ij} = stress-tensor components, psi
σ_{kk} = normal-stress summation, psi
σ_n = normal stress to fracture plane, psi
σ_v = vertical in-situ stress, psi
ς = fracture spacing, ft
ϕ_m = phase porosity

Acknowledgments

The authors are thankful to the Tulsa University Drilling Research Projects (TUDRP) member companies for their technical and financial support. They also thank N. Takach for his helpful comments and reviews.

References

Aadnøy, B. S. 2010. *Modern Well Design*, second edition. New York City: CRS Press.

Abousleiman, Y. and Nguyen, V. 2005. Poromechanics Response of Inclined Wellbore Geometry in Fractured Porous Media. *J. Eng. Mech.* **131** (11): 1170–1183. https://doi.org/10.1061/(ASCE)0733-9399(2005)131:11(1170).

Aifantis, E. C. 1979. On the Response of Fissured Rocks. *Develop. Mech.* **10:** 249–253.

API SPEC 13A, Specification for Drilling Fluid Materials, 18th edition. 2010. Washington, DC: API.

Ashley, P. R. 2000. Well Control of an Influx From a Fracture Breathing Formation. Presented at the IADC/SPE Asia Pacific Drilling Technology, Kuala Lumpur, 11–13 September. SPE-62770-MS. https://doi.org/10.2118/62770-MS.

Babu, D. R. 1998. Effect of P–ρ–T Behavior of Muds on Loss/Gain During High-Temperature Deep-Well Drilling. *J. Pet. Sci. Eng.* **20** (1–2): 49–62. https://doi.org/10.1016/S0920-4105(98)00003-5.

Bai, M., Abousleiman, Y., Cui, L. et al. 1999. Dual-Porosity Poroelastic Modeling of Generalized Plane Strain. *Int. J. Rock Mech. Min.* **36** (8): 1087–1094. https://doi.org/10.1016/S1365-1609(99)00065-9.

Barenblatt, G. I. and Zheltov, Y. P. 1960. Fundamental Equations of Filtration of Homogeneous Liquids in Fissured Rocks. *Soviet Phys. Doklady* **5:** 522.

Bear, J., Tsang, C.-F., and de Marsily, G. 2012. *Flow and Contaminant Transport in Fractured Rock*. San Diego, California: Academic Press.

Belfield, W. C. and Sovich, J. P. 1995. Fracture Statistics From Horizontal Wellbores. *J Can Pet Technol* **34** (6): 47–50. PETSOC-95-06-04. https://doi.org/10.2118/95-06-04.

Berryman, J. G. and Wang, H. F. 1995. The Elastic Coefficients of Double-Porosity Models for Fluid Transport in Jointed Rock. *J. Geophys. Res.-Sol. Ea.* **100** (B12): 24611–24627. https://doi.org/10.1029/95JB02161.

Biot, M. A. 1941. General Theory of Three-Dimensional Consolidation. *J. Appl. Phys.* **12** (2): 155–164. https://doi.org/10.1063/1.1712886.

Biot, M. A. 1956. General Solutions of the Equations of Elasticity and Consolidation for a Porous Material. *J. Appl. Mech.* **23** (1): 91–96.

Biot, M. A. and Willis, D. G. 1957. The Elastic Coefficients of the Theory of Consolidation. *J. Appl. Mech.* **24:** 594–601.

Biryukov, D. and Kuchuk, F. J. 2012. Transient Pressure Behavior of Reservoirs With Discrete Conductive Faults and Fractures. *Transport Porous Med.* **95** (1): 239–268. https://doi.org/10.1007/s11242-012-0041-x.

Bour, O. and Davy, P. 1997. Connectivity of Random Fault Networks Following a Power Law Fault Length Distribution. *Water Resour. Res.* **33** (7): 1567–1583. https://doi.org/10.1029/96WR00433.

Bruel, D., Cacas, M. C., Ledoux, E. et al. 1994. Modelling Storage Behaviour in a Fractured Rock Mass. *J. Hydrol.* **162** (3–4): 267–278. https://doi.org/10.1016/0022-1694(94)90231-3.

Cheng, A. H.-D. 2016. *Poroelasticity, Theory and Applications of Transport in Porous Media*, Vol. 27. Cham, Switzerland: Springer International Publishing.

Cinelli, G. 1965. An Extension of the Finite Hankel Transform and Applications. *Int. J. Eng. Sci.* **3** (5): 539–559. https://doi.org/10.1016/0020-7225(65)90034-0.

Detournay, E. and Carvalho, J. L. 1989. Application of the Pressurized Hollow Poroelastic Cylinder Solution To the Interpretation of Laboratory Burst Experiments. Presented at the 30th US Symposium on Rock Mechanics, Morgantown, West Virginia, 19–22 June. ARMA-89-0377.

Dyke, C. G., Wu, B., and Milton-Tayler, D. 1995. Advances in Characterising Natural Fracture Permeability From Mud Log Data. *SPE Form Eval* **10** (3): 160–166. SPE-25022-PA. https://doi.org/10.2118/25022-PA.

Elsworth, D. and Bai, M. 1992. Flow-Deformation Response of Dual-Porosity Media. *J. Geotech. Eng.* **118** (1): 107–124. https://doi.org/10.1061/(ASCE)0733-9410(1992)118:1(107).

Feng, Y. and Gray, K. E. 2017. Modeling Lost Circulation Through Drilling-Induced Fractures. *SPE J.* **23** (1): 205–223. SPE-187945-PA. https://doi.org/10.2118/187945-PA.

Gill, J. A. 1989. How Borehole Ballooning Alters Drilling Responses. *Oil Gas J.* **87** (11): 41–45.

Hart, D. J. and Wang, H. F. 1995. Laboratory Measurements of a Complete Set of Poroelastic Moduli for Berea Sandstone and Indiana Limestone. *J. Geophys. Res.-Sol. Ea.* **100** (B9): 17741–17751. https://doi.org/10.1029/95JB01242.

Helstrup, O. A., Rahman, M. K., Hossain, M. M. et al. 2001. A Practical Method for Evaluating Effects of Fracture Charging and/or Ballooning When Drilling High Pressure, High Temperature (HPHT) Wells. Presented at the SPE/IADC Drilling Conference, Amsterdam, 27 February–1 March. SPE-67780-MS. https://doi.org/10.2118/67780-MS.

Helstrup, O. A., Rahman, K., Chen, Z. et al. 2003. Poroelastic Effects on Borehole Ballooning in Naturally Fractured Formations. Presented at the SPE/IADC Drilling Conference, Amsterdam, 19–21 February. SPE-79849-MS. https://doi.org/10.2118/79849-MS.

Jones, F. O. Jr. 1975. A Laboratory Study of the Effects of Confining Pressure on Fracture Flow and Storage Capacity in Carbonate Rocks. *J Pet Technol* **27** (1): 21–27. SPE-4569-PA. https://doi.org/10.2118/4569-PA.

Karstad, E. 1998. Analysis of Ballooning Effects During Drilling of High Pressure High Temperature Wells. Presented at the European Petroleum Conference, The Hague, 20–22 October. SPE-52066-STU. https://doi.org/10.2118/52066-STU.

Khaled, M. Y., Beskos, D. E., and Aifantis, E. C. 1984. On the Theory of Consolidation With Double Porosity—III. A Finite Element Formulation. *Int. J. Numer. Anal. Meth. Geomech.* **8** (2): 101–123. https://doi.org/10.1002/nag.1610080202.

Kuchuk, F. and Biryukov, D. 2015. Pressure-Transient Tests and Flow Regimes in Fractured Reservoirs. *SPE Res Eval & Eng* **18** (2): 187–204. SPE-166296-PA. https://doi.org/10.2118/166296-PA.

Kuchuk, F., Biryukov, D., and Fitzpatrick, T. 2015. Fractured-Reservoir Modeling and Interpretation. *SPE J.* **20** (5): 983–1004. SPE-176030-PA. https://doi.org/10.2118/176030-PA.

Lavrov, A. and Tronvoll, J. 2003. Mud Loss Into a Single Fracture During Drilling of Petroleum Wells: Modeling Approach. *Proc.,* Development and Application of Discontinuous Modelling for Rock Engineering, 6th International Conference ICADD-6, Trondheim, Norway, 5–8 October, 189–198.

Lavrov, A. and Tronvoll, J. 2004. Modeling Mud Loss in Fractured Formations. Presented at the Abu Dhabi International Conference and Exhibition, Abu Dhabi, 10–13 October. SPE-88700-MS. https://doi.org/10.2118/88700-MS.

Lavrov, A. and Tronvoll, J. 2005. Mechanics of Borehole Ballooning in Naturally-Fractured Formations. Presented at the SPE Middle East Oil and Gas Show and Conference, Bahrain, 12–15 March. SPE-93747-MS. https://doi.org/10.2118/93747-MS.

Lavrov, A. and Tronvoll, J. 2006. Numerical Analysis of Radial Flow in a Natural Fracture: Applications in Drilling Performance and Reservoir Characterization. Presented at the Abu Dhabi International Petroleum Exhibition and Conference, Abu Dhabi, 5–8 November. SPE-103564-MS. https://doi.org/10.2118/103564-MS.

Lietard, O., Unwin, T., Guillot, D. et al. 1996. Fracture Width LWD and Drilling Mud/LCM Selection Guidelines in Naturally Fractured Reservoirs. Presented at the European Petroleum Conference, Milan, Italy, 22–24 October. SPE-36832-MS. https://doi.org/10.2118/36832-MS.

Majidi, R., Miska, S. Z., Yu, M. et al. 2008. Fracture Ballooning in Naturally Fractured Formations: Mechanism and Controlling Factors. Presented at the SPE Annual Technical Conference and Exhibition, Denver, 21–24 September. SPE-115526-MS. https://doi.org/10.2118/115526-MS.

Majidi, R., Miska, S., Thompson, L. G. et al. 2010. Quantitative Analysis of Mud Losses in Naturally Fractured Reservoirs: The Effect of Rheology. *SPE Drill & Compl* **25** (4): 509–517. SPE-114130-PA. https://doi.org/10.2118/114130-PA.

Majidi, R., Edwards, S., Zhang, J. et al. 2015. Drilling Depleted Sands: Geomechanics, Challenges and Mitigations. Presented at the SPE Annual Technical Conference and Exhibition, Houston, 28–30 September. SPE-174741-MS. https://doi.org/10.2118/174741-MS.

Marbun, B. T. H., Widiyanto, Y. A., and Kurnianto, B. E. 2014. Feasibility Study of Casing While Drilling Application on Geothermal Drilling Operation. Oral presentation given at the Thirty-Ninth Workshop on Geothermal Reservoir Engineering, Stanford, California, 24–26 February.

Miska, S. Z., Samuel, G. R., and Azar, J. J. 1998. Modeling of Pressure Buildup on a Kicking Well and Its Practical Application (includes associated paper 56853). *SPE Drill & Compl* **13** (4): 207–213. SPE-52884-PA. https://doi.org/10.2118/52884-PA.

Muskat, M. 1934. The Flow of Compressible Fluids Through Porous Media and Some Problems in Heat Conduction. *Physics* **5** (3): 71–94. https://doi.org/10.1063/1.1745233.

Muskat, M. 1949. *Physical Principles of Oil Production.* New York City: McGraw-Hill.

Ochoa Lugo, A. J., Acevedo, O. D., Nieto, L. et al. 2011. Successful Application of MPD (Managed Pressure Drilling) for Prevention, Control, and Detection of Borehole Ballooning in Tight Gas Reservoir in Cuervito Field, Mexico. Presented at the Canadian Unconventional Resources Conference, Calgary, 15–17 November. SPE-146529-MS. https://doi.org/10.2118/146529-MS.

Ozdemirtas, M., Babadagli, T., and Kuru, E. 2009. Experimental and Numerical Investigations of Borehole Ballooning in Rough Fractures. *SPE Drill & Compl* **24** (2): 256–265. SPE-110121-PA. https://doi.org/10.2118/110121-PA.

Power, D., Ivan, C. D., and Brooks, S. W. 2003. The Top 10 Lost Circulation Concerns in Deepwater Drilling. Presented at the SPE Latin American and Caribbean Petroleum Engineering Conference, Port-of-Spain, Trinidad and Tobago, 27–30 April. SPE-81133-MS. https://doi.org/10.2118/81133-MS.

Rice, J. R. and Cleary, M. P. 1976. Some Basic Stress Diffusion Solutions for Fluid-Saturated Elastic Porous Media With Compressible Constituents. *Rev. Geophys.* **14** (2): 227–241. https://doi.org/10.1029/RG014i002p00227.

Ridley, K. M., Jurgens, M., Billa, R. J. et al. 2013. Eagle Ford Shale Well Control: Drilling and Tripping in Unconventional Oil and Gas Plays. Presented at the SPE Unconventional Gas Conference and Exhibition, Muscat, Oman, 28–30 January. SPE-163984-MS. https://doi.org/10.2118/163984-MS.

Rosenberg, S. M. and Gala, D. M. M. 2011. Liner Drilling Technology as a Mitigation To Wellbore Ballooning—A Successful Case Study in the Gulf of Mexico Shelf. Presented at the SPE/IADC Drilling Conference and Exhibition, Amsterdam, 1–3 March. SPE-140261-MS. https://doi.org/10.2118/140261-MS.

Sadd, M. H. 2009. *Elasticity: Theory, Applications, and Numerics*. Cambridge, Massachusetts: Academic Press.

Sanfillippo, F., Brignoli, M., Santarelli, F. J. et al. 1997. Characterization of Conductive Fractures While Drilling. Presented at the SPE European Formation Damage Conference, The Hague, 2–3 June. SPE-38177-MS. https://doi.org/10.2118/38177-MS.

Schmitt, D. R., Tait, R. J., and Spann, H. 1993. Solution for Pore Pressure and Stress in a Porous Hollow Cylinder: Application To a Laboratory Experiment. *Int. J. Rock Mech. Min.* **30** (7): 1057–1060. https://doi.org/10.1016/0148-9062(93)90071.

Sneddon, I. N. 1995. *Fourier Transforms*. North Chelmsford, Massachusetts: Courier Corporation.

Tare, U. A., Whitfill, D. L., and Mody, F. K. 2001. Drilling Fluid Losses and Gains: Case Histories and Practical Solutions. Presented at the SPE Annual Technical Conference and Exhibition, New Orleans, 30 September–3 October. SPE-71368-MS. https://doi.org/10.2118/71368-MS.

Tarr, B. A., Ladendorf, D. W., Sanchez, D. et al. 2016. Next-Generation Kick Detection During Connections: Influx Detection at Pumps Stop (IDAPS) Software. *SPE Drill & Compl* **31** (4): 250–260. SPE-178821-PA. https://doi.org/10.2118/178821-PA.

Terzaghi, K. 1923. Die Berechnung der Durchlassigkeitsziffer des Tones aus dem Verlauf der Hydrodynamischen Spannungserscheinungen. *Sitzungsber. Akad. Wiss. Math. Naturwiss. Kl. Abt.* **132** (2A): 105–124.

Tirado Vargas, G. R., Lupo, C. P. M., Beltran, J. C. et al. 2011. MPD Makes Possible To Drill and Trip Out of the Hole in a Gas Well With a Combination of a Narrow Mud Weight Window and a Serious Ballooning Effect. Presented at the IADC/SPE Managed Pressure Drilling and Underbalanced Operations Conference & Exhibition, Denver, 5–6 April. SPE-143104-MS. https://doi.org/10.2118/143104-MS.

Valliappan, S. and Khalili-Naghadeh, N. 1990. Flow Through Fissured Porous Media With Deformable Matrix. *Int. J. Numer. Meth. Eng.* **29** (5): 1079–1094. https://doi.org/10.1002/nme.1620290512.

Van Everdingen, A. F. and Hurst, W. 1949. The Application of the Laplace Transformation To Flow Problems in Reservoirs. *J Pet Technol* **1** (12): 305–324. SPE-949305-G. https://doi.org/10.2118/949305-G.

Verga, F. M., Carugo, C., Chelini, V. et al. 2000. Detection and Characterization of Fractures in Naturally Fractured Reservoirs. Presented at the SPE Annual Technical Conference and Exhibition, Dallas, 1–4 October. SPE-63266-MS. https://doi.org/10.2118/63266-MS.

Ward, C. and Clark, R. 1998. Anatomy of a Ballooning Borehole Using PWD Tool. *Proc.,* 3rd Workshop on Overpressures in Petroleum Exploration, Pau, France, 7–8.

Warren, J. E. and Root, P. J. 1963. The Behavior of Naturally Fractured Reservoirs. *SPE J.* **3** (3): 245–255. SPE-426-PA. https://doi.org/10.2118/426-PA.

Watson, G. N. 1922. *A Treatise on the Theory of Bessel Functions*. Cambridge, UK: Cambridge University Press.

Wilson, R. K. and Aifantis, E. C. 1982. On the Theory of Consolidation With Double Porosity. *Int. J. Eng. Sci.* **20** (9): 1009–1035. https://doi.org/10.1016/0020-7225(82)90036-2.

Yuan, Z., Morrell, D., Mayans, A. G. et al. 2016. Differentiate Drilling Fluid Thermal Expansion, Wellbore Ballooning and Real Kick During Flow Check With an Innovative Combination of Transient Simulation and Pumps Off Annular Pressure While Drilling. Presented at the IADC/SPE Drilling Conference and Exhibition, Fort Worth, Texas, 1–3 March. SPE-178835-MS. https://doi.org/10.2118/178835-MS.

Zimmerman, R. W. and Bodvarsson, G. S. 1996. Hydraulic Conductivity of Rock Fractures. *Transport Porous Med.* **23** (1): 1–30. https://doi.org/10.1007/BF00145263.

Appendix A—Dual-Porosity Constitutive Model

Berryman and Wang (1995) proposed a new constitutive framework for dual-porosity media. Because of the choice of independent variables in Eq. A-1, the following is referred to as the stress formulation.

$$\begin{pmatrix} \delta\varepsilon_{kk} \\ -\delta\zeta_1 \\ -\delta\zeta_2 \end{pmatrix} = \frac{1}{K}\begin{pmatrix} 1 & -\overline{\alpha}_1 & -\overline{\alpha}_2 \\ -\overline{\alpha}_1 & \overline{\alpha}_1/B_{u1} & Ka_{23} \\ -\overline{\alpha}_2 & Ka_{23} & \overline{\alpha}_2/B_{u2} \end{pmatrix}\begin{pmatrix} -\delta\sigma_{kk} \\ -\delta p_1 \\ -\delta p_2 \end{pmatrix}, \quad \text{(A-1)}$$

where K is the overall bulk modulus and B_{u1} and B_{u2} are the generalized Skempton coefficients (Berryman and Wang 1995) for the case of drained matrix/undrained fractures and drained fractures/undrained matrix, respectively. The coefficient a_{23} is the cross-storage coefficient. These coefficients can be expressed as functions of fluid, pore, and fracture properties as (Berryman and Wang 1995)

$$B_{u2} = B_2 \text{ and } B_{u1} = \frac{v_1/K_1}{[v_1(1/K_f + 1/K_1)]},$$

$$K = \left(\frac{v_1}{K_1} + \frac{v_2}{K_2}\right)^{-1},$$

$$\overline{\alpha}_1 = \frac{(1/K - 1/K_{u1})}{B_{u1}K} \text{ and } K_{u1} = \left[\frac{1}{K} + \left(\frac{v_1}{K_1}\right)^2 \frac{1}{v_1(1/K_f + 1/K_1)}\right]^{-1}$$

$$\overline{\alpha}_2 = \frac{(1/K - 1/K_{u2})}{B_{u2}K} \text{ and } K_{u1} = \left[\frac{1}{K} + \left(\frac{v_2\alpha_2}{K_2}\right)^2 \frac{B_2K_2}{v_2\alpha_2}\right]^{-1}, \quad \text{(A-2)}$$

where K_f, K_1, and K_2 are the fluid, fracture, and matrix bulk moduli, respectively; B_2 and α_2 are the classical Skempton and Biot and Willis (1957) coefficients of the porous matrix (Cheng 2016); ν_1 and ν_2 are the volume fractions; and K_{u1} and K_{u2} are the generalized bulk moduli for the case of drained pores/undrained fractures and drained fractures/undrained pores, respectively.

Appendix B—Solution of the Coupled Diffusion Problem

The general Sturm-Liouville (Sneddon 1995) problem answers to

$$\frac{\mathrm{d}^2 f}{\mathrm{d}x^2}+\frac{1}{x}\frac{\mathrm{d}f}{\mathrm{d}x}-\frac{v^2}{x^2}f=0, \quad \alpha \le x \le b, \qquad \text{(B-1)}$$

where α and b are the inner and outer boundaries, respectively. If the boundary conditions are the same as in Eqs. 16a and 16b, then we have (Cinelli 1965)

$$\begin{cases} f(a) = \text{Dirichlet condition} \\ f'(b) = \text{Neumann condition.} \end{cases} \qquad \text{(B-2)}$$

The general solution to Eq. B-1 is

$$f(x) = AJ_v(\xi_n x) + BY_v(\xi_n x), \qquad \text{(B-3)}$$

where ξ_n is the positive roots of the transcendental equation (Cinelli 1965),

$$J_v(\xi_n \alpha)Y'_v(\xi_n b) - Y_v(\xi_n \alpha)J'_v(\xi_n b) = 0. \qquad \text{(B-4)}$$

In Eq. B-3, J_v and Y_v are the Bessel functions of the first and second kind, respectively, of order v (Watson 1922). Now, depending on the applicable boundary conditions, the Hankel transform pair can be derived (Cinelli 1965),

$$\overline{f}_H(\xi_n) = H[f(x)] = \int_a^b xf(x)[J_\nu(\xi_n x)Y'_v(\xi_n b) - Y_\nu(\xi_n x)J'_v(\xi_n b)]\mathrm{d}x. \qquad \text{(B-5)}$$

Eq. B-5 defines the Hankel transform of $f(x)$.

$$f(x) = \frac{\pi^2}{2}\sum_{\xi_n}\frac{\xi_n^2 J_\nu^2(\xi_n a)\overline{f}_H(\xi_n)}{\{[1-(\nu/\xi_n b)^2]J_\nu^2(\xi_n a) - [J'_v(\xi_n b)]^2\}}[J_\nu(\xi_n x)Y_v{}'(\xi_n b) - Y_\nu(\xi_n x)J'_v(\xi_n b)]. \qquad \text{(B-6)}$$

Finally, it follows that the original Sturm-Liouville equation can be reduced to (Cinelli 1965)

$$H\left(\frac{\mathrm{d}^2 f}{\mathrm{d}x^2}+\frac{1}{x}\frac{\mathrm{d}f}{\mathrm{d}x}-\frac{\nu^2}{x^2}f\right) = \frac{2}{\pi\xi_n}f'(b) - \frac{2}{\pi}\frac{J'_v(\xi_n b)}{J_\nu(\xi_n a)}f(a) - \xi_n^2\overline{f}_H(\xi_n). \qquad \text{(B-7)}$$

With reference to this problem, and in particular to Eq. 14a, it can be realized that the appropriate version of the Sturm-Liouville equation requires the parameter $v = 0$. This means that the resulting finite Hankel transform pair would be defined as

$$\begin{aligned} \overline{p}_H(\xi_n) &= H[p(r)] = \int_a^b rf(r)[J_1(\xi_n b)Y_0(\xi_n r) - Y_1(\xi_n b)J_0(\xi_n r)]\mathrm{d}r, \\ p(r) &= \frac{\pi^2}{2}\sum_{\xi_n}\frac{\xi_n^2[J_0(\xi_n a)]^2\overline{f}_H(\xi_n)}{\{J_0^2(\xi_n a) - [-J_1(\xi_n b)]^2\}}[J_1(\xi_n b)Y_0(\xi_n r) - Y_1(\xi_n b)J_0(\xi_n r)], \end{aligned} \qquad \text{(B-8)}$$

with ξ_n being the positive roots of the transcendental equation

$$J_1(\xi_n b)Y_0(\xi_n a) - Y_1(\xi_n b)J_0(\xi_n a) = 0. \qquad \text{(B-9)}$$

By applying the Hankel transform given in Eq. B-5 and the property in Eq. B-7, it is possible to reduce Eqs. 14a and 14b into a system of ordinary differential equations (ODEs):

$$\begin{aligned} &\frac{1}{C_{11}}\frac{\partial\overline{p}_1}{\partial t}+\frac{1}{C_{12}}\frac{\partial\overline{p}_2}{\partial t} = -\xi_n^2\overline{p}_1 + \frac{2}{\pi}\frac{J_1(\xi_n b)}{J_0(\xi_n a)}p_w, \\ &\frac{1}{C_{21}}\frac{\partial\overline{p}_1}{\partial t}+\frac{1}{C_{22}}\frac{\partial\overline{p}_2}{\partial t} = 0. \end{aligned} \qquad \text{(B-10)}$$

To solve the system of Eq. B-10, it is first necessary to decouple it, and this passage is achieved by diagonalization. By introducing the new variable u such that

$$\overline{p}_m = Lu_m \text{ and } L = \begin{bmatrix} -C_{21}/C_{22} & 0 \\ 1 & 1 \end{bmatrix}, \qquad \text{(B-11)}$$

the system of Eq. B-10 can be diagonalized to

$$\begin{bmatrix}\dot{u}_1\\ \dot{u}_2\end{bmatrix}=\begin{bmatrix}-C_{11}^{*}\xi_n^2 & 0\\ 0 & 0\end{bmatrix}\begin{bmatrix}u_1\\ u_2\end{bmatrix}+\begin{bmatrix}-\dfrac{2}{\pi}\dfrac{J_1(\xi_n b)}{J_0(\xi_n a)}p_w C_{21}^{*}\\ 0\end{bmatrix}, \quad \text{(B-12)}$$

where

$$C_{11}^{*}=\frac{C_{11}C_{12}C_{21}}{C_{12}C_{21}-C_{11}C_{22}},$$
$$C_{21}^{*}=\frac{C_{11}C_{12}C_{22}}{C_{11}C_{22}-C_{12}C_{21}}. \quad \text{(B-13)}$$

Eq. B-12 is a system of decoupled ODEs. Considering saturated void spaces with initial pressures in Eq. 16, the solution for such a system can be written as

$$\begin{cases} u_2(\xi_n,t)=u_2(r,0),\\ u_1(\xi_n,t)=\dfrac{C_{22}}{C_{21}}\dfrac{2}{\pi\xi_n^2}p_w\dfrac{J_1(\xi_n b)}{J_0(\xi_n a)}(e^{-C_{11}^{*}\xi_n^2 t}-1)+e^{-C_{11}^{*}\xi_n^2 t}u_1(r,0). \end{cases} \quad \text{(B-14)}$$

To solve the ODEs in the system of Eq. B-12, an expression for the initial conditions in terms of the new variable u_m is needed. Hence, it follows that

$$u_m(r,0)=u_m^0=V^{-1}\overline{p}_{H,m}^0=\begin{bmatrix}-\overline{p}_{H,1}^0\dfrac{C_{22}}{C_{21}}\\ \overline{p}_{H,2}^0+\overline{p}_{H,1}^0\dfrac{C_{22}}{C_{21}}\end{bmatrix}, \quad \text{(B-15)}$$

where the transformed initial pressures read

$$\overline{p}_{H,m}^0=\int_a^b rp_m^0[J_1(\xi_n b)Y_0(\xi_n r)-Y_1(\xi_n b)J_0(\xi_n r)]\mathrm{d}r. \quad \text{(B-16)}$$

The general solution for the system of Eq. B-12 is the sum of the solutions in Eq. B-14,

$$u(\xi_n,t)=u_1(\xi_n,t)+u_2(\xi_n,t). \quad \text{(B-17)}$$

Moving back to the transformed pressure, by applying Eq. B-11,

$$\overline{p}_m(\xi_n,t)=\left[\frac{2}{\pi}p_w\frac{C_{22}}{C_{21}}(e^{-C_{11}^{*}\xi_n^2 t}-1)+e^{-C_{11}^{*}\xi_n^2 t}u_1^0\right]\begin{bmatrix}-C_{21}/C_{22}\\ 1\end{bmatrix}+u_2^0\begin{bmatrix}0\\ 1\end{bmatrix}. \quad \text{(B-18)}$$

The pressure distribution in the fractures and the pores can finally be found by expanding the products in Eq. B-18. This gives the pressure distribution in the Hankel transform space.

$$\begin{cases} \overline{p}_{H,1}=-\dfrac{C_{21}}{C_{22}}\left\{\left[-\overline{p}_{H,1}^0\dfrac{C_{22}}{C_{21}}+\dfrac{C_{22}}{C_{21}}\dfrac{2}{\pi\xi_n^2}p_w\dfrac{J_1(\xi_n b)}{J_0(\xi_n a)}\right]e^{-C_{11}^{*}\xi_n^2 t}-\dfrac{C_{22}}{C_{21}}\dfrac{2}{\pi\xi_n^2}p_w\dfrac{J_1(\xi_n b)}{J_0(\xi_n a)}\right\},\\ \overline{p}_{H,2}=\left[-\overline{p}_{H,1}^0\dfrac{C_{22}}{C_{21}}+\dfrac{C_{22}}{C_{21}}\dfrac{2}{\pi\xi_n^2}p_w\dfrac{J_1(\xi_n b)}{J_0(\xi_n a)}\right]e^{-C_{11}^{*}\xi_n^2 t}-\dfrac{C_{22}}{C_{21}}\dfrac{2}{\pi\xi_n^2}p_w\dfrac{J_1(\xi_n b)}{J_0(\xi_n a)}+\overline{p}_{H,2}^0+\overline{p}_{H,1}^0\dfrac{C_{22}}{C_{21}}. \end{cases} \quad \text{(B-19)}$$

Now, before proceeding with the inversion to the real-space domain, it is convenient to explicitly express the initial conditions. This can be done by considering Eq. B-16. Defining the function

$$U(\xi_n r)=J_1(\xi_n b)Y_0(\xi_n r)-Y_1(\xi_n b)J_0(\xi_n r), \quad \text{(B-20)}$$

with reference to Watson (1922), we can use the identity

$$\int_a^b rU(\xi_n r)\mathrm{d}r=-\frac{1}{{\xi_n}^2}\left(r\frac{\mathrm{d}U}{\mathrm{d}r}\right)_a^b. \quad \text{(B-21)}$$

The derivatives of the U function evaluated at the two radii read

$$\begin{cases} U'(\xi_n b)=0,\\ U'(\xi_n a)=\dfrac{2}{\pi a}\dfrac{J_1(\xi_n b)}{J_0(\xi_n a)}. \end{cases} \quad \text{(B-22)}$$

Eventually, a formulation for the transformed initial conditions is found as

$$\overline{p}^{0}_{H,m} = \int_a^b p^0_m r U(\xi_n r)\mathrm{d}r = -\frac{1}{{\xi_n}^2}\frac{2}{\pi a}\frac{J_1(\xi_n b)}{J_0(\xi_n a)}p^0_m. \quad \text{(B-23)}$$

By substituting Eq. B-23 into Eq. B-19 and rearranging, the expressions for the pressures in the Hankel domain are obtained as

$$\begin{cases} \overline{p}_{H,1} = \dfrac{2}{\pi\xi_n^2}\dfrac{J_1(\xi_n b)}{J_0(\xi_n a)}[(p^0_1 - p_w)e^{-C^*_{11}\xi_n^2 t} + p_w], \\ \overline{p}_{H,2} = \dfrac{2}{\pi\xi_n^2}\dfrac{J_1(\xi_n b)}{J_0(\xi_n a)}\left[\dfrac{C_{22}}{C_{21}}(1 - e^{-C^*_{11}\xi_n^2 t})(p^0_1 - p_w) + p^0_2\right]. \end{cases} \quad \text{(B-24)}$$

The following step would be to transform the pressure distributions evaluated in Eq. B-24 to the real-space domain using the inversion formula given by Eq. B-8.

SI Metric Conversion Factors

bbl × 1.5898	E−01 = m^3
cp × 1.0*	E−03 = Pa·s
gal/min × 6.31	E−05 = m^3/s
psi × 6.8947	E+03 = Pa
md × 9.8692	E−16 = m^2
lbm/gal × 1.1982	E+02 = kg/m^3
in. × 2.54*	E−02 = m
ft × 3.048*	E−01 = m

*Conversion factor is exact.

Silvio Baldino is currently a PhD-degree candidate in petroleum engineering at the University of Tulsa (TU) and a research assistant at TUDRP. He is conducting research on well control, geomechanics, and drilling-fluid rheological characterization. Before starting his PhD degree studies, Baldino worked as a project manager for Flowserve Corporation in the engineered-centrifugal-pumps division. He is a recipient of the 2017 Outstanding Reviewer Award for the *Journal of Petroleum Science and Engineering*. Baldino has been an SPE member since 2013. He holds bachelor's and master's degrees in energy engineering from the Polytechnic University of Milan, Italy.

Stefan Z. Miska is currently the Jonathan Detwiler Endowed Chair Professor of the McDougall School of Petroleum Engineering and an associate director of TUDRP at TU. Over the years, he has taught at his alma mater, the University of Mining and Metallurgy, Poland; the Norwegian Institute of Technology; and the New Mexico Institute of Mining and Technology. Miska was involved in the successful design and development of a downhole, turbine-type motor for air drilling and has been instrumental in the development of research facilities for wellbore hydraulics at simulated downhole conditions. He also has made contributions to the development of new buckling concepts and the axial-force transfer in extended-reach drilling. Miska's current research interests are focused on geomechanics, mechanics of tubulars, and wellbore hydraulics. He holds master's and PhD degrees from the University of Mining and Metallurgy. Miska is an SPE Distinguished Member and the recipient of the 2000 SPE Award for Distinguished Petroleum Engineering Faculty and the 2004 SPE Drilling Engineering Award, and achieved SPE/AIME Honorary Membership status in 2018. He was recently awarded the title of professor of technical sciences by the president of Poland.

Evren M. Ozbayoglu is currently the Chapman Endowed Wellspring Associate Professor of Petroleum Engineering at TU, and the director of TUDRP. Previously, he was a faculty member at the Middle East Technical University, Turkey. Ozbayoglu has participated in several industrial projects on major drilling-engineering topics, including wellbore hydraulics, hole cleaning, tubular mechanics, and fluid rheological characterization. He holds bachelor's and master's degrees from the Middle East Technical University and a PhD degree from TU. Ozbayogu has been an SPE member since 1994 and an American Society of Mechanical Engineers member since 2015. He is a recipient of the 2012 SPE Outstanding Technical Editor Award for *SPE Journal*, the 2013 SPE Outstanding Technical Editor Award for *SPE Reservoir Evaluation & Engineering*, the 2015 SPE Outstanding Technical Editor Award for *SPE Drilling & Completion*, and the 2013 SPE Regional Distinguished Faculty Award for the Mid Continent Region.